Optimizing surfactant templating of yttria-stabilized zirconia aerogels for high-temperature applications: Effect of anionic and nonionic surfactant

Rebecca C. Walker,[†] Kimberly E. Penzer,[†] Jamesa L. Stokes,[‡] Frances I. Hurwitz,[‡,¶] Haiquan Guo,[§] and James K. Ferri[*,†]

[†]*Department of Chemical & Life Science Engineering, Virginia Commonwealth University, Richmond, VA*

[‡]*NASA Glenn Research Center, Cleveland, OH*

[¶]*Retired*

[§]*Universities Space Research Association, Cleveland, OH*

E-mail: jkferri@vcu.edu

Abstract

Aerogels, mesoporous materials with extreme material properties including high specific surface area, low density, and low thermal conductivity, can be useful for applications including catalysis, sorption media, and drug delivery. The low thermal conductivity and high surface area of aerogels makes them advantageous as thermal management systems, specifically for aerospace or aeronautics applications. However, the pore collapse and subsequent surface area decrease of aerogels following exposure to high temperatures must be mitigated to allow aerogels to be effectively used in thermal management applications. This work investigates the anionic surfactant sodium dodecyl sulfate (SDS) and the nonionic surfactant Pluronic® P-123 as surfactant templates in yttria-stabilized zirconia (YSZ) aerogels. By utilizing surfactant templates, known to influence pore structure, it is anticipated that sintering and densification of the aerogels following high-temperature exposure will be mitigated. It was determined that the addition of SDS and P-123 increased the surface area and pore volume of as-dried aerogels and suppressed crystallite growth at high temperatures. However, the impact of surfactant templates on the surface area and pore volume of heat-treated aerogels was negligible, potentially due to low concentrations of surfactant and the removal of the surfactant following high-temperature exposure.

Keywords

Yttria-stabilized zirconia aerogels; mesoporous structure; anionic surfactant templating; nonionic surfactant templating; material optimization

1 Introduction

Aerogels are unique, highly porous materials with a wide variety of extreme material properties, including high specific surface area, low density, and low thermal conductivity. Aerogels, first introduced in 1932, are gels which have been isolated from their liquid component, as a gas replaces all of the gel's liquid through a drying process [1]. Aerogels are composed of 95 - 99% air by volume and are the lightest solid material in the world [2]. Due to their material properties, aerogels can be useful in a range of applications, such as catalysis, thermoresisters, sorption media, sensors, electrodes in solid oxide fuel cells, and drug delivery [3–9]. The high specific surface area and low thermal conductivity enables the effective use of aerogels as thermal management systems [10–13]. Zirconia (ZrO_2) aerogels have special interest for high-temperature applications due to the high melting point of ZrO_2 (2715°C) and stability between 600°C and 1000°C, where other aerogel systems, such as silica, often begin to sinter and densify. To further increase the thermal stability of zirconia aerogels, yttria-stabilized zirconia (YSZ) aerogels are often used as the addition of yttrium to the zirconia system stabilizes high temperature polymorphs of zirconia. However, exposure of YSZ aerogels to high-temperature often leads to pore structure collapse and surface area decrease due to structural rearrangement and polycondensation reactions [14, 15]. Pore structure collapse increases the thermal conductivity of the aerogels, inhibiting their use at high-temperature; therefore, to effectively use aerogels in thermal management systems, collapse of pore structure and decrease of surface area must be mitigated.

To influence the pore structure of aerogels, surfactants can be used as templating agents during aerogel synthesis. Surfactants are used in the synthesis of a variety of aerogels as these chemicals can be used as structure directing agents to influence pore structure in mesoporous materials due to electrostatic repulsion and steric hinderance effects [3, 16]. Surfactants can template the aerogel structure during synthesis, enhancing surface area and pore size upon high-temperature exposure [17–19]. With a hydrophilic head and a hy-

drophobic tail, surfactants can reduce interfacial energy, which causes surface tension in the aerogel system and leads to pore collapse and shrinkage during drying [20, 21]. Surfactants control nanoparticle and crystallite growth through a capping effect, which influences crystalline structure; they also prevent agglomeration, which increases aerogel surface area.

The surfactant templating process is depicted in Scheme 1. Various surfactants form micelles, either spherical or rod-like in shape, at or above the surfactant's critical micelle concentration (CMC) [22]. Surfactants are added to the sol prior to gelation, as aerogel precursor particles aggregate around the micelles. Following the addition of a gelation agent, gelation occurs and the precursor particles form a solid network around the micelles. The presence of the surfactants typically does not impede the formation of the solid gel matrix [23]. The surfactants are oxidized and removed from the aerogel system following washing or high-temperature exposure, either through the drying process or heat-treatment, resulting in uniform pores [24]. Surfactants are not required for the synthesis of aerogels, as the aerogel porosity primarily results from the aggregation of the precursor and formation of the solid gel network. However, it is anticipated that surfactant templating can be used to influence the aerogel pore structure, enabling the retention of mesoporous structure and high surface area in aerogels.

In prior work, we used the cationic (positively charged) surfactant cetrimonium bromide, CTAB, as a templating agent for 20 mol% yttria-stabilized zirconia (YSZ) aerogels [24]. As compared to aerogels without CTAB, it was determined that 0.5x the CMC of CTAB increased the surface area of YSZ aerogels by 72% and 41% following high-temperature exposure to 600°C and 1000°C, respectively. Additionally, at 0.5x CTAB, the aerogel pore volume was shown to increase by 75% and 80% at 600°C and 1000°C, respectively. When compared to a concentration of 2x the CMC of CTAB, the concentration of 0.5x had a greater increase in surface area and pore volume. We hypothesized that the higher concentration of CTAB may have negatively influenced gelation of the YSZ sol due to adsorption of the cationic surfactant onto the charged surface sites of the zirconia matrix and subse-

quent impediment to gelation. This may have decreased the strength of the YSZ gel, leading to increased shrinkage during drying and heat-treatment, and ultimately causing pore collapse and surface area reduction.

To determine the effect of surfactants with different charges on the pore structure of aerogels, we consider anionic (negatively charged) and nonionic (without charge) surfactants as templates for 20 mol% YSZ aerogels in this work. The anionic surfactant sodium dodecyl sulfate (SDS) and the nonionic surfactant Pluronic® P-123 were chosen as templating agents for YSZ aerogels. SDS, a well-known organic sodium salt, has been used as a surfactant template for materials such as ambient-pressure dried silica aerogels and highly porous ceramic zirconia foams, while the linear tri-block-copolymer P-123 has been reported as a templating agent in aerogels including ambient-pressure dried zirconia aerogels and titania-silica aerogels. The addition of each templating agent led to an increase in surface area, pore volume, and thermal stability[21, 23, 25–29]. In this work, the surfactants were added to the aerogels at concentrations of 0.5x, 2x, and 3x the CMC of each surfactant to understand the influence of surfactant type and concentration; the aerogels were heat-treated at temperatures up to 1100°C to determine the effect of the surfactants on the thermal stability of the aerogels. It was anticipated that the use of SDS and P-123 as surfactant templates would enable the retention of mesoporous structure and high surface area in as-dried aerogels, while also mitigating crystallite growth and densification of aerogels exposed to high-temperatures.

2 Experimental

2.1 Yttria-stabilized zirconia (YSZ) aerogel synthesis

Yttria-stabilized zirconia (YSZ) aerogels were synthesized using a similar sol-gel procedure to the one used by Hurwitz et al [30]. Zirconyl chloride octahydrate, $ZrOCl_2 \cdot 8\,H_2O$ (12.374 g/38.40 mmol, Alfa Aesar, 99.9% metals basis), and yttrium(III) chloride hexahydrate, $YCl_3 \cdot 6\,H_2O$ (2.912 g/9.60 mmol, Acros Organics, 99.9%) were used as the zirco-

nium and yttrium precursors, respectively. The precursors were mixed at room temperature with the solvent system, ethanol (38 mL per 48 mmol of total solids, Decon Labs, 200 proof) and deionized water (6.572 mL/365 mmol), to create the sol. To minimize experimental variables, a yttria content of 20 mol% was chosen for the formulations as this yttria content was shown to retain mesoporous structure and increase thermal stability after high-temperature exposure compared to lower dopant levels [30, 31]. Regarding water content, twice the stoichiometric amount (2x water) was chosen, as this water level resulted in aerogels with greater surface area and pore volume at high temperature than higher water levels following experimentation.

Prior to gelation, the surfactants chosen for this study, sodium dodecyl sulfate, SDS (Sigma Aldrich, ACS reagent, $\geq$ 99.0%) or Pluronic® P-123 (Sigma-Aldrich, average M_n $\sim$5,800) were added to the sol as a multiple (0.5x, 2x,and 3x) of the surfactant's critical micelle concentration (CMC), the determination of which is discussed in section 2.2. Aerogels without surfactant were also synthesized for comparison. The sol was mixed overnight to allow for complete dissolution of the surfactants and precursors. Propylene oxide (8 mL/114 mmol, Sigma Aldrich, ReagentPlus, 99%), was used as a gelation agent. Following further mixing of the sol in an ice bath, the gelation agent was added to the chilled sol. Immediately after the addition of propylene oxide, the sol was poured into cylindrical molds with gelation typically occurring within 2 - 5 minutes. After aging for 24 hours, the gel was washed in 200 proof ethanol for 5-8 days. The gel was then supercritically dried using carbon dioxide. The supercritical drying process exchanged the solvent in the gel's pores with air, transforming the gel into an aerogel. Following drying, the aerogels were heat-treated in high-purity alumina boats under flowing argon at temperatures of 600°C, 1000°C, and 1100°C for 18 min. The ramp rate of the tube furnace was 5°C/min.

2.2 Predictive measurements for surfactants

Prior to the synthesis of the YSZ aerogels, the concentration of each surfactant that would be added to the aerogels was determined. The surfactants were to be added as multiples (0.5x, 2x, and 3x) of the surfactant's critical micelle concentration (CMC) value in the YSZ aerogel sol. The CMC value was determined using a series of experiments where different concentrations of each surfactant were added prior to gelation to the base sol, which was the 20 mol% yttria, 2x water YSZ sol formulation used for all of the aerogels in this work. The hydrodynamic radius of each solution was determined using dynamic light scattering on an ALV/CGS-3 Compact Goniometer from ALV-GmbH utilizing a vertically polarized 633 nm 22 mW laser.

For SDS, there was a correlation between hydrodynamic radius value and surfactant concentration as seen in Figure 1A. The hydrodynamic radius values were between 3.7 and 4.6 nm for SDS concentrations between 1 x 10^{-5} M and 1 x 10^{-2} M in the base sol. SDS concentrations above 1 x 10^{-2} M were not measured as SDS would not dissolve into the base sol, even with extended mixing times (> 3 days). Theta (θ), defined as (R - R_{min})/(R_{max} - R_{min}) where R is the hydrodynamic radius, was plotted as a function of the concentration of SDS in the base sol solution. The CMC of SDS was determined to be 50% of the θ value; therefore, the CMC was determined to be 1 x 10^{-3} M in the aerogel base sol, denoted by the red dashed line in Figure 1A. This estimated value of the SDS CMC in the base sol (an ethanol-water solvent system) was reasonable, as the CMC of SDS in water at 25°C is 8 x 10^{-3}; the CMC is known to increase with the addition of ethanol, but decrease with the addition of salts, such as the inorganic zirconium and yttrium precursors [32, 33]. For the aerogel formulations discussed in section 2.1, at 0x, 0.5x, 2x, and 3x the CMC of SDS, the CMC value of 1 x 10^{-3} M SDS was used; the molar ratios of SDS to inorganic precursors in the aerogel formulations are given in Table 1.

For the surfactant P-123, the hydrodynamic radius values ranged from 3.6 nm to 4.8 nm for P-123 concentrations between 5 x 10^{-6} and 1 x 10^{-2} M P-123 in the base sol. How-

ever, there was no correlation between θ and surfactant concentration as seen in Figure 1B. Therefore, as a benchmark, the CMC of P-123 in water, a value of 3 x 10^{-4} M, was used for the aerogel formulations discussed in section 2.1 [34]. The molar ratios of P-123 to inorganic precursors in the aerogel formulations are given in Table 1. It should be noted that, between 5 x 10^{-2} M P-123 and 1 x 10^{-1} M P-123, there was a large increase seen in hydrodynamic radius value from 7.67 nm to 22.02 nm. YSZ aerogels were made with a concentration of 1 x 10^{-1} M P-123, equaling approximately 320x the CMC of P-123, although with relatively low surface area compared to the aerogels synthesized with other P-123 concentrations; therefore, this concentration was not included in the following discussion.

In this work, we mapped a predictive measurement, surfactant hydrodynamic radius, in the sol to final properties of the synthesized aerogels. It was anticipated that a predictive measurement that can be made in the sol, prior to gelation, drying, heat-treatment and characterization, could save experimental time and resources by providing insight into final aerogel properties before completion of the full aerogel synthetic pathway.

2.3 Characterization

Following synthesis, as-dried and heat-treated aerogels were characterized using a variety of techniques. As-dried shrinkage and density were determined through physical measurement using a digital caliper. Scanning electron microscopy was performed using a Hitachi S-4700 FE-SEM to show, qualitatively, the effects of surfactant on microstructure. The SEM samples were uncoated and imaged at 2 kV with a working distance of 5.0 - 9.0 mm. Nitrogen physisorption was conducted on a Tristar II 3020 (Micrometrics Instrument Corporation) instrument following degas at 80°C overnight; surface area of the aerogels was determined using the Brunauer–Emmett–Teller (BET) method and the pore size distribution was determined from the desorption isotherm using the Barrett-Joyner-Halenda (BJH) method, which accounts for open pores less than 100 nm in size only [35, 36]. Fol-

lowing the measurement, pore size distributions of the aerogel samples were determined by plotting the pore volume (cm^3/g) as a function of the pore diameter (nm). A Bruker D8 Advance X-ray diffractometer was used to determine surfactant effects on crystalline phase transformation and average crystallite size for heat-treated aerogels. Cu Kα (1.54059 Å) radiation was used from 10° to 80° 2θ. Profile fitting in HighScore Plus by Malvern Panalytical was used to analyze the aerogel samples. To determine the average crystallite size for each sample, the Scherrer equation, the Monshi-Scherrer (M-S) method, the Williamson-Hall (W-H) method, and the Size-Strain-Plot (SSP) method were used [37]. Transmission electron microscopy was conducted using a FEI Talos TEM to confirm the effects of surfactant on crystallite size.

3 Results and discussion

3.1 As-dried shrinkage & density

Following supercritical drying, physical measurements were taken to determine the as-dried shrinkage (%) and density (g/cm^3) for the synthesized YSZ aerogels. The as-dried shrinkage was a measure of the percent change between the aerogel monolith following supercritical drying and the syringe mold used during synthesis. For aerogels without surfactant, the as-dried shrinkage was 17% and the density was 0.254 g/cm^3. For aerogels with SDS, the as-dried shrinkage and density remained approximately constant for the various amounts of SDS at 17% and 0.248 g/cm^3, respectively. The addition of SDS as a templating agent had a negligible effect on the as-dried shrinkage and density, as compared to aerogels without SDS. For aerogels with P-123, the as-dried shrinkage and density remained approximately constant at 16% and at 0.229 g/cm^3 for varying surfactant levels. The as-dried shrinkage and density were slightly lower for aerogels synthesized using P-123 than for aerogels synthesized with SDS or synthesized without a templating agent. The density was shown to decrease by 10% for aerogels with P-123 as compared to aerogels without templating agent. This decrease in density may have been due to the high

molecular weight of P-123, approximately 5800 g/mol, which was much higher than the molecular weight of SDS at 288.38 g/mol. As some of the surfactant was likely removed from the aerogel system during drying due to washing via the supercritical solvents, aerogels synthesized with the higher molecular weight surfactant P-123 may have resulted in a lower density as-dried aerogel as compared to aerogels with SDS or without a templating agent.

3.2 Pore structure

Figure 2 shows scanning electron microscopy (SEM) images at 80kx magnification representing YSZ aerogels with no templating agent (Figure 2A), with 3x SDS (Figure 2B), and with 3x P-123 (Figure 2C) at four different heat-treatment conditions of as-dried, 600°C, 1000°C, and 1100°C.

Sintering was expected following high-temperature exposure due to polycondensation reactions and structural rearrangement; sintering often leads to pore collapse and densification of the pore structure. In Figure 2, the aerogels kept the mesoporous structure at 1000°C, however densification of the aerogel pore structure was evident following exposure to 1100°C. Exposure to 1100°C resulted in larger voids present in the SDS and P-123 templated aerogel samples.

Regarding surfactant influence on the aerogel pore structure, differences in the aerogel pore structure between aerogels without a templating agent (Figure 2A), aerogels with SDS (Figure 2B), and aerogels with P-123 (Figure 2C) were difficult to distinguish from SEM micrographs. The as-dried aerogel with SDS (Figure 2B) did display a few larger voids that were not present in the as-dried aerogels without surfactant template and with P-123. However, there was difficulty in assigning statistical significance to the shifts in pore size.

3.3 Pore size distributions

The pore size distributions for as-dried and heat-treated at 1000°C YSZ aerogels are displayed in Figure 3 for SDS (Figure 3A,C) and P-123 (Figure 3B,D).

In the as-dried aerogels with SDS and the as-dried aerogels with P-123, the measured pore sizes were larger than the average diameter of both the SDS micelles and the P-123 micelles measured in the YSZ aerogel sol. However, the pores were not all directly formed by the surfactant micelles as the surfactants only aided in pore templating. The primary mechanism for the formation of aerogel pores was the aggregation of the solid precursor and the resultant arrangement of the gel network.

For as-dried aerogels with SDS, the major pore size distributions were centered around 32 nm for all SDS concentrations. These pore sizes were slightly larger compared to the as-dried aerogel without SDS, which had a major pore size distribution centered around 28 nm. The addition of SDS promoted slightly larger pore sizes and volumes, possibly indicating that SDS was an effective surfactant template. The aerogel without templating agent had the widest pore size distribution, from 0 nm to 93 nm, as compared to the aerogels with SDS, which had pore size distributions from 0 to 45 nm (0.5x SDS), 0 to 52 nm (2x SDS), and 0 to 42 nm (3x SDS). Surfactants are known to increase the emulsification of the sol and prevent particle agglomeration, leading to a more homogeneous aerogel [21]. The addition of SDS led to a narrower pore size distribution for the as-dried aerogels by potentially increasing the homogeneity of the pores. The presence of macropores was not evident in the as-dried pore size distributions for the aerogels with SDS. Larger pores were present in the as-dried aerogel without a surfactant template, which could have potentially encouraged the collision of air molecules, ultimately increasing the thermal conductivity. For the aerogels heat-treated at 1000°C, the pore size distributions were very similar in the aerogel without SDS and the aerogels with 2x and 3x SDS. For the aerogel with 0.5x SDS heat-treated at 1000°C, the pore size distribution was wider and macropores were present.

For as-dried aerogels with P-123, the addition of higher concentrations of P-123 ap-

peared to shift the major pore size distributions to slightly larger pore sizes. In the as-dried aerogel without P-123 (0x P-123), the major pore size distribution was centered around 28 nm, which shifted to slightly higher pore sizes centered around 40 nm at 2x P-123 and 35 nm at 3x P-123. However, at a smaller concentration of P-123 (0.5x P-123), the major pore size was slightly smaller at 18 nm than in the aerogel without a templating agent. Larger pore sizes occurred only above the critical micelle concentration (CMC) of P-123, potentially indicating that only the presence of micelles led to larger pores in the as-dried aerogels with P-123 surfactant templates. Aerogels with P-123 had overall wide pore size distributions, from 0 nm to 78 nm at 0.5x P-123 and from 0 nm to 95 nm at 2x P-123, which were approximately equal to the pore size distribution in the aerogel without templating agent (0x P-123) at 0 nm to 93 nm. The large pore size distribution may have resulted from the large size of the P-123 surfactant template. For the aerogel with 3x P-123, the pore size distribution was narrower from 0 nm to 42 nm, which indicated the presence of mesopores only. However, the presence of macropores in the as-dried aerogels with lower concentrations of P-123 may have increased the thermal conductivity of the aerogels due to increased air molecule collisions. For the aerogels heat-treated at 1000°C, the pore size distributions were very similar in the aerogel without P-123 and the aerogels with P-123.

When comparing the different surfactants, at 0.5x CMC, the as-dried major pore size was larger in the aerogel with SDS (32 nm) as compared to the aerogel with P-123 (18 nm). However, there was a larger volume of pores at 32 nm for the aerogel with SDS than pores at 18 nm for the aerogel with P-123, which had a much wider pore size distribution. For higher concentrations of surfactant, the as-dried major pore size was similar between the aerogels with SDS and the aerogels with P-123. At 2x CMC, the major pore size was 32 nm in the aerogel with SDS and centered around 40 nm, but with a much wider pore size distribution, in the aerogel with P-123. At 3x CMC, the major pore size was slightly smaller in the aerogel with SDS (32 nm) than in the aerogel with P-123 (35 nm). At lower

concentrations, it seemed that SDS was a more effective surfactant template, leading to larger mesopores (pores between 2 and 50 nm); at higher concentrations, SDS and P-123 led to pores with similar pore sizes. The as-dried aerogels with P-123 did contain macropores (pores > 50 nm) at 0.5x P-123 and 2x P-123, while the as-dried aerogels with SDS were primarily mesoporous. Due to a narrower pore size distribution, SDS may have been more effective in emulsification of the aerogel sol, leading to aerogels with more homogeneous pore structure than the aerogels with P-123. The as-dried aerogels with P-123 may have had a wider pore size distribution due to the larger size of the P-123 surfactant templates, as compared to the SDS surfactant templates.

To maintain effectiveness as a thermal insulator, the formation of large pores should be mitigated. Small mesopores inhibit gas convection as the pore diameter is small compared to the mean free gas path, which can hinder the collision of gas molecules. For the as-dried aerogels with P-123, the presence of pores greater than 50 nm and wider pore size distribution may have resulted in increased gas convection due to increased opportunity for gas molecule collisions. The larger volume of mesopores in the as-dried aerogels with SDS would have potentially lowered the thermal conductivity of these aerogels as compared to the aerogels with P-123 due to suppression of gas convection. Enhanced control of the mesopore range in aerogels with SDS may have resulted from increased electrostatic interactions present in the aerogels with the anionic surfactant template as compared to the aerogel with the nonionic surfactant template.

It is important to note that nitrogen physisorption is only capable of measuring pores less than 100 nm. Therefore, pores with diameters greater than 100 nm could have been present in the synthesized as-dried aerogels. While there was no evident macroporosity (pores > 50 nm) observed in the as-dried SEM micrographs for the aerogel without a surfactant template (Figure 2A) and the aerogel with 3x P-123 (Figure 2C), a few larger voids were observed in the as-dried aerogel with 3x SDS (Figure 2B). For this sample, while a significant volume of pores with diameters less than 50 nm were observed in the

pore size distribution (Figure 3A), the aerogel could have had pores greater than 100 nm that were not measured through nitrogen physisorption. For the aerogels heat-treated at 1000°C, mesoporosity was retained; however, pores greater than 100 nm could have also been present.

3.4 Surface area & pore volume

The BET surface area (m^2/g) values, with BJH desorption cumulative pore volume (cm^3/g) values in the inset, are represented in Figure 4A for aerogels with SDS and Figure 4B for aerogels with P-123. The error of BET surface area is within 10 - 20 m^2/g based on repeat measurements.

For all aerogels represented, there was a large decrease in both surface area and pore volume following high-temperature exposure. A decrease in surface area and pore volume was expected due to the sintering and densification of the aerogel pore structure at high-temperatures. The larger voids were not included in the measurement of the surface area and pore volume values displayed in Figure 4 since nitrogen physisorption was only capable of measuring pores less than 100 nm. However, the surface area and pore volume values at high-temperature, although much lower than the as-dried values, still indicated the retention of mesoporosity following high-temperature exposure. The retention of mesoporosity was also shown in the pore size distribution plots following high-temperature exposure (Figure 3C,D).

For as-dried aerogels with SDS, 0.5x SDS and 3x SDS had higher BET surface area values, at 445 m^2/g and 449 m^2/g, respectively than 2x SDS at 413 m^2/g. All concentrations of SDS had higher surface areas than the aerogel without a surfactant template, with a surface area of 379 m^2/g. For the heat-treated aerogels, the aerogels with SDS and the aerogels without SDS all had approximately the same surface area value, with a difference of 17 m^2/g between the aerogels with or without SDS at 600°C, a difference of 16 m^2/g between the aerogels at 1000°C, and a negligible difference of 4 m^2/g between the aerogels at

1100°C.

The as-dried aerogels with P-123 all had higher surface areas, at 436 m^2/g, 453 m^2/g, and 423 m^2/g for 0.5x P-123, 2x P-123, and 3x P-123, respectively, than the aerogel without a surfactant template at 379 m^2/g. Similar to aerogels with SDS, for the heat-treated aerogels, the aerogels with P-123 and the aerogels without P-123 all had approximately the same surface area value, with a difference of 19 m^2/g between the aerogels with or without P-123 at 600°C, a difference of 19 m^2/g between the aerogels at 1000°C, and a difference of 17 m^2/g between the aerogels at 1100°C. It should be noted that at 600°C, the aerogel without P-123 had the higher surface area of 156 m^2/g than the surface areas at 140 m^2/g, 140 m^2/g, and 137 m^2/g of the aerogels at 0.5x P-123, 2x P-123, and 3x P-123, respectively.

The BET surface area of as-dried aerogels demonstrated an increase when using both SDS and P-123 as surfactant templates at various concentrations. There was a negligible difference in the as-dried surface areas of aerogels with SDS and the surface areas of aerogels with P-123. Both surfactants were effective templates indicated by a higher surface area than the aerogel without the surfactant template. It was determined that, following high-temperature exposure, the use of a surfactant template did not have a strong impact on aerogel surface area, as the differences in surface areas between aerogels without a surfactant template and aerogels with SDS or P-123 were negligible.

Regarding the BJH desorption cumulative pore volume values, the as-dried aerogels using SDS as a surfactant template had a higher pore volume, at 2.00 cm^3/g, 1.62 cm^3/g, and 1.71 cm^3/g for 0.5x SDS, 2x SDS, and 3x SDS, respectively, as compared to the aerogel without a surfactant template at 1.39 cm^3/g. As was the case with BET surface area, the larger pore volume in as-dried aerogels with SDS indicated that SDS potentially was an effective surfactant template. At 600°C, the aerogel without SDS and the aerogel with 0.5x SDS both had higher pore volume, both at 1.01 cm^3/g, than the aerogels with higher surfactant content (2x SDS and 3x SDS) with pore volumes at 0.72 cm^3/g. Following heat-

treatment at 1000°C and 1100°C, the pore volumes were approximately the same for aerogels without a surfactant template and aerogels with SDS with a variation of 0.1 cm^3/g and 0.03 cm^3/g, respectively. For as-dried aerogels with P-123 as a surfactant template, the aerogel with the lowest surfactant concentration, 0.5x P-123, had the lowest pore volume at 0.97 cm^3/g, while the aerogel with the highest surfactant concentration, 3x P-123, had the highest pore volume at 1.62 cm^3/g. At 600°C, similar to SDS, the aerogel without a surfactant template had the highest pore volume at 1.01 cm^3/g, as compared to the aerogels with 0.5x P-123, 2x P-123, and 3x P-123 at 0.90 cm^3/g, 0.85 cm^3/g, and 0.81 cm^3/g, respectively. For aerogels heat-treated at 1000°C and 1100°C, the pore volumes were approximately the same in aerogels without a surfactant template and aerogels with P-123; the variation of pore volume was 0.20 cm^3/g at 1000°C and 0.17 cm^3/g at 1100°C.

The as-dried pore volumes were slightly larger for aerogels with SDS, as compared to the aerogels with P-123 as the surfactant template. The increased electrostatic interactions of the anionic surfactant with the aerogel matrix may have increased the as-dried pore volume of the aerogels with SDS. Additionally, due to the higher molecular weight of P-123 as compared to SDS, larger amounts of P-123 surfactant may have been retained in the aerogel pore structure following the washing and drying processes; this may have resulted in smaller pore volumes for the as-dried aerogels with P-123 as compared to the as-dried aerogels with SDS surfactant templates. The addition of SDS also increased the pore volume of as-dried aerogels as compared to the aerogel without a surfactant template. Some concentrations of P-123 increased the as-dried pore volume as compared to the aerogel without a surfactant template, although the increase was not as large as when SDS was used. However, similar to the results for BET surface area, following high-temperature exposure, the addition of SDS or P-123 did not significantly enhance the aerogel pore volume.

3.5 Crystalline structure

X-ray diffraction (XRD) was used to determine the effect of concentrations of SDS and P-123 on the crystalline structure of YSZ aerogels. The resulting XRD patterns from 10° to 80° 2θ are displayed in Figure 5. For aerogels without a templating agent, patterns are displayed for the aerogel heat-treated at 600°C, 1000°C, and 1100°C. For aerogels at 0.5x SDS, 3x SDS, 0.5x P-123, and 3x P-123, patterns at 1100°C only are displayed.

All synthesized as-dried aerogels, regardless of the presence or absence of SDS or P-123 surfactant templates, were non-crystalline or amorphous. However, all heat-treated aerogels exhibited crystallinity, which increased with increasing heat-treatment temperature, indicated by the presence of well-defined peaks in the XRD pattern. Following analysis, it was determined that all heat-treated YSZ aerogels exhibited the cubic fluorite crystalline phase, regardless of surfactant concentration; the cubic phase is expected in 20 mol% yttria YSZ aerogels up to 2500°C [38]. The use of SDS and P-123 as surfactant templates was found to have no effect on the resulting crystalline structure of the YSZ aerogels.

Table 2 displays the average crystallite size (Å) values for each aerogel sample at 600°C, 1000°C, and 1100°C. For the XRD analysis, the crystallite size values resulting from four different equations, the Scherrer equation, the Monshi-Scherrer (M-S) method, the Williamson-Hall (W-H) method, and the Size-Strain-Plot (SSP) method, were averaged [37]. These four equations were used together, as the Scherrer equation, traditionally used to determine crystallite size, has restrictions above 1000 Å and often has error due to noise and instrument signal. Due to the limitations and errors associated with the XRD equations, analysis of images from transmission electron microscopy (TEM) was also used to confirm the average crystallite size.

Crystallite growth was evident following high-temperature exposure, especially at 1000°C and 1100°C. This was expected as high-temperature is known to increase growth of crystallite particles, promoting crystallization. At 1000°C, the average crystallite size determined via XRD analysis was slightly lower in all aerogels with SDS than the aerogel with-

out a surfactant template; 2x SDS exhibited the lowest average crystallite size for aerogels with SDS at 197 ± 11 Å. The aerogels with P-123 at 1000°C also all had a lower average crystallite size than the aerogel without a surfactant template, with 3x P-123 having the lowest crystallite size at 198 ± 5 Å.

At 1100°C, there was a different behavior as the aerogel without the surfactant template had a slightly smaller average crystallite size of 529 ± 39 Å than the aerogels with SDS, which had average crystallite sizes ranging from 535 Å to 605 Å. For aerogels with P-123, the average crystallite size in the aerogels with 0.5x and 3x P-123 was lower than the crystallite size in the aerogel without a surfactant template at 349 ± 3 Å and 517± 32 Å, respectively. At 2x P-123, the average crystallite size was larger at 579 ± 18 Å. The presence of P-123 mitigated crystallite growth at 0.5x P-123 and 3x P-123; however, for aerogels with SDS and for the aerogel at 2x P-123, the crystallite size increased as compared to the aerogel without a surfactant template.

At 1000°C, the presence of SDS and P-123 surfactant templates was shown to decrease the average crystallite size compared to the aerogel without a surfactant template. Due to a capping effect, surfactants are known to control crystallite growth; the lower average crystallite size at 1000°C potentially indicated that SDS and P-123 were effective surfactant templates, inhibiting crystallite growth at this high temperature. At 1100°C, the SEM micrographs (Figure 2) displayed significant densification, which was even more pronounced than in the aerogels heat-treated at 1000°C. Increased densification was potentially indicative of a decrease in the effectiveness of SDS and P-123 as surfactant templates, which was further evidenced by a negligible impact of the surfactants on the surface area and pore volume of the aerogels at 1100°C. The greater extent of densification and the insignificant impact on the crystallite size at 1100°C may have indicated that SDS and P-123 were more effective surfactant templates at 1000°C than at 1100°C.

The TEM images are displayed for aerogels with no templating agent (Figure 6A), with 0.5x SDS (Figure 6B), with 0.5x P-123 (Figure 6C), with 3x SDS (Figure 6D), and

with 3x P-123 (Figure 6E) that were heat-treated at 1100°C. The TEM images are displayed at 58kx magnification.

In Figure 6, it can be seen that crystallite particles with a distribution of sizes were present in all of the aerogel samples; differences in the TEM images were difficult to distinguish. The crystallite size values at 1100°C determined via TEM analysis in Table 2 were all approximately the same, ranging from 347 Å to 364 Å, except for the aerogel with 0.5x SDS which was higher at 411 Å. The average crystallite size values determined via TEM were lower than the crystallite size values determined via XRD. However, the standard deviations were large, between 128 Å and 176 Å. These large standard deviations resulted from the wide variations in size of the crystallite particles in the TEM images (Figure 6). Figure 7 includes the distribution of crystallite sizes displayed in the TEM images. The size distribution was very broad for all of the samples. The larger particles in Figure 6 could have been agglomerates of multiple crystallites, attributing to the broad size distribution. It should be noted that for the aerogels with a surfactant template, both at 0.5x and 3x, the major crystallite size distributions were slightly smaller than for the aerogel without a surfactant template, potentially demonstrating that adding the surfactant template may have suppressed crystallite growth even at 1100°C.

3.6 Comparison of surfactants

At or above the critical micelle concentration (CMC), SDS forms micelles which can embed in the aerogel network through reactions involving hydroxyl groups [26]. The embedded SDS micelles could have influenced the aerogel pore structure through steric hinderance effects, as well as through electrostatic interactions between the metal ions of the aerogel network and the negatively charged surfactant head groups. Similar to a cationic surfactant, anionic surfactants also release ions when dissolved in solution that could have interacted with the zirconia aerogel matrix, inducing a repulsive force between the zirconia particles. These electrostatic interactions, while not the only means of anionic surfactant

templating, were a significant influence on aerogel pore formation.

Regarding the nonionic surfactant, Pluronic® P-123 is a linear tri-block-copolymer, forming core-shell micelles at or above the CMC [39]. While charged surfactant micelles can embed into the zirconia aerogel matrix through electrostatic interactions, nonionic surfactants form hydrogen bonds between the zirconia aerogel matrix and the ether oxygens of the surfactant [21, 40, 41]. Nonionic surfactants also do not release ions; with nonionic surfactant templating, pore structure was primarily influenced by the hydrogen bonding and steric hinderance effects of the surfactant micelles resulting from the nonionic surfactant interaction with the zirconia aerogel matrix. In the aerogels with the nonionic P-123, electrostatic interactions were not prevalent; therefore, the increased electrostatic interactions in the aerogels with SDS may have been the driving force behind the enhanced pore structure control, evidenced by the formation of primarily mesopores with narrower size distributions and increased cumulative pore volumes in as-dried aerogels. However, more experimental work may be needed to further understand the surfactant templating mechanisms and the interactions between the surfactants and the zirconia aerogel matrix.

Both SDS and P-123 increased the surface area of as-dried aerogels as compared to the aerogel without a surfactant template. The increase in surface area for the as-dried aerogels may have been indicative of higher threshold operating limits for the surfactant-templated aerogels. However, increased surface area was not demonstrated following high-temperature exposure at 600°C, 1000°C, and 1100°C. Above temperatures of 350°C, the surfactants were most likely oxidized and removed from the aerogel system [24]. Since the maximum temperature for the supercritical drying process stayed below 100°C in this work, remnants of surfactant not removed during the washing process were most likely still present in the as-dried aerogels; however, during the heat-treatment process, well above 350°C, any remaining surfactant was removed [30]. The presence of remaining surfactant in the as-dried aerogels templated with SDS and P-123 may have influenced the higher as-dried surface area, and the higher pore volume in the case of SDS templated aerogels.

However, following exposure to temperatures above 600°C and full removal of surfactant from the aerogel system, the surface area and pore volume of the aerogels with SDS and P-123 showed negligible differences when compared to the aerogels without surfactant template. The advantages, reduction of pore collapse and mitigation of densification, of the anionic and nonionic surfactant templates were mostly eliminated following the removal of the surfactants. This was further evidenced by the inhibition of crystallite growth at 1000°C, which was not as apparent at 1100°C. At higher temperatures, the advantages of the surfactant templates were diminished.

The behavior of surfactant-templated aerogels was much different for the aerogels templated with SDS (anionic surfactant) and P-123 (nonionic surfactant) as compared to prior work using cetrimonium bromide, CTAB (cationic surfactant), as a template. A concentration of 0.5x CTAB increased the surface area of YSZ aerogels by 72% and 41% following exposure to 600°C and 1000°C, respectively, as compared to aerogels without CTAB [24]. Pore volume was also shown to increase at 0.5x CTAB by 75% and 80% at 600°C and 1000°C, respectively. CTAB was shown to increase surface area and pore volume in heat-treated aerogels, however, at 0.5x CTAB, the as-dried surface area was 403 m^2/g, lower than any of the as-dried aerogels using SDS and P-123 surfactant templates. Therefore, while SDS and P-123 increased the as-dried surface area as compared to CTAB, there was not an enhancement of surface area and pore volume at high-temperature for these surfactants as there was for CTAB.

We hypothesize two reasons for the different behavior in the cationic surfactant templated aerogels: the estimation of the CMC value for CTAB and the strong interaction of the CTAB surfactant with the zirconia aerogel matrix. First, prior to the gelation of the YSZ aerogels, CTAB was added in multiples of 0.5x and 2x the CMC of CTAB. Unlike with the anionic and nonionic surfactants, where the CMC was estimated from a literature value or experimental measurements (Figure 1), the value of CTAB used in the aerogel formulations was estimated from a thermodynamic model [42]. This thermodynamic model

only considered the water and ethanol volumes in the sol and did not take into account other factors, including the inorganic salt concentration. Due to this estimation, the molar ratios of CTAB and the inorganic precursors in the aerogel formulation were high (0.13 for 0.5x CTAB and 0.50 for 2x CTAB) compared to the molar ratios of SDS and P-123 (Table 1). While there may have been problems with the estimation of the CTAB CMC, the larger amount of CTAB in the YSZ aerogels may have had a larger influence on the aerogel pore structure, in both as-dried and heat-treated aerogel samples, as compared to the SDS and P-123 templated aerogels.

However, the larger amount of CTAB potentially had negative effects on the aerogel pore structure. As discussed previously, larger amounts of CTAB (2x the CMC as compared to 0.5x the CMC) resulted in lower surface areas and pore volumes of as-dried and heat-treated aerogels. It was hypothesized that the higher concentration of CTAB led to increased adsorption and a potential build-up of the surfactant onto the zirconia aerogel matrix, which could have impeded the gelation reaction and caused subsequent shrinkage and pore collapse during drying and heat-treatment. Therefore, while higher amounts of CTAB may have positively influenced the surface area and pore volume of aerogels as compared to the lower amounts of SDS and P-123, too much CTAB was shown to have a negative impact.

Regarding aerogels with SDS and P-123, larger amounts of both surfactants may have positively impacted the surface area and pore volume of surfactant templated aerogels at high-temperature. Larger concentrations of micelles, as well as increased electrostatic interactions in aerogels with SDS, could have further decreased surface tension and prevented agglomeration, leading to reduced pore collapse and higher surface area. However, increased amounts of surfactants may have potentially led to an excess of surfactant, causing gelation impediment due to matrix adsorption in the case of SDS or due to steric effects in the case of P-123 that could have resulted in negative impacts to surface area and pore volume.

4 Conclusions

In this work, we synthesized YSZ aerogels using the anionic surfactant, sodium dodecyl sulfate (SDS), and the nonionic surfactant, Pluronic® P-123. We anticipated that surfactant templates would enhance surface area and pore volume and mitigate high-temperature sintering and densification of the aerogels. We also demonstrated the use of a predictive measurement, surfactant hydrodynamic radius, to map the behavior of surfactants in the sol prior to gelation to the final properties of YSZ aerogels, potentially saving experimental time.

For as-dried aerogels, it was determined that SDS and P-123 were effective surfactant templates, increasing the surface area, pore volume, and pore size of YSZ aerogels, as compared to aerogels without a surfactant template. The anionic surfactant SDS led to primarily mesopores in as-dried aerogels, while certain concentrations of the nonionic surfactant P-123 led to the formation of macropores. This may have been due to increased electrostatic interactions between the ions of SDS and the zirconia aerogel matrix, leading to more control over pore formation. Aerogels with SDS also had narrower pore size distributions, which could have indicated that SDS increased the homogeneity of the aerogel pore structure. Following high-temperature exposure, the use of SDS and P-123 surfactant templates did not have an influence on the aerogel surface area, pore volume, or crystalline phase. However, at 1000°C, aerogels with SDS and P-123 had smaller average crystallite sizes than the aerogel without a surfactant template, indicative of the control of crystallite growth by the surfactants via a capping effect. At 1100°C, the addition of SDS did not decrease crystallite size, although some concentrations of P-123 did decrease crystallite size. This may have indicated that SDS and P-123 were more effective surfactant templates at 1000°C than 1100°C, further evidenced by increased densification of the pore structure at 1100°C. At higher temperatures, the advantages of SDS and P-123 as surfactant templates may have diminished. We expect that further optimization of the aerogel formulation us-

ing surfactant templates will enable the effective use of YSZ aerogels at temperatures up to 1100°C.

Acknowledgements

The authors would like to acknowledge Dr. Anita Garg (NASA Glenn Research Center) for TEM imaging. R.C.W. would like to acknowledge National Aeronautics and Space Administration (NASA) Fellowship 80NSSC18K1697 for financial support of this work.

References

(1) Aegerter, M.; Leventis, N.; Koebel, M. *Aerogels Handbook*; Springer New York, 2011; DOI: 10.1007/978-1-4419-7589-8.

(2) Smirnova, I.; Gurikov, P. Aerogel production: Current status, research directions, and future opportunities. *J. Supercrit. Fluids* **2018**, *134*, 228–233, DOI: 10.1016/j.supflu.2017.12.037.

(3) Bangi, U. K. H.; Park, H.-H. Evolution of textural characteristics of surfactant-mediated mesoporous zirconia aerogel powders prepared via ambient pressure drying route. *Int. Nano Lett.* **2018**, *8*, 221–228, DOI: 10.1007/s40089-018-0241-7.

(4) Feinle, A.; Hüsing, N. Mixed metal oxide aerogels from tailor-made precursors. *J. Supercrit. Fluids* **2015**, *106*, 2–8, DOI: 10.1016/j.supflu.2015.07.015.

(5) Lee, Y.; Choi, J. W.; Suh, D. J.; Ha, J. M.; Lee, C. H. Ketonization of hexanoic acid to diesel-blendable 6-undecanone on the stable zirconia aerogel catalyst. *Appl. Catal., A* **2015**, *506*, 288–293, DOI: 10.1016/j.apcata.2015.09.008.

(6) Liu, B.; Gao, M.; Liu, X.; Xie, Y.; Yi, X.; Zhu, L.; Wang, X.; Shen, X. Monolithic zirconia aerogel from polyacetylacetonatozirconium precursor and ammonia hydroxide gel initiator: formation mechanism, mechanical strength and thermal properties. *RSC Adv.* **2018**, *8*, 41603–41611, DOI: 10.1039/C8RA08263D.

(7) Maleki, H. Recent advances in aerogels for environmental remediation applications: A review. *Chemical Engineering Journal* **2016**, *300*, 98–118, DOI: 10.1016/j.cej.2016.04.098.

(8) Stergar, J.; Maver, U. Review of aerogel-based materials in biomedical applications. *J. Sol-Gel Sci. Technol.* **2016**, *77*, 738–752, DOI: 10.1007/s10971-016-3968-5.

(9) Ulker, Z.; Erkey, C. An emerging platform for drug delivery: Aerogel based systems. *J. Controlled Release* **2014**, *177*, 51–63, DOI: 10.1016/j.jconrel.2013.12.033.

(10) Koebel, M.; Rigacci, A.; Achard, P. Aerogel-based thermal superinsulation: An overview. *J. Sol-Gel Sci. Technol.* **2012**, *63*, 315–339, DOI: 10.1007/s10971-012-2792-9.

(11) Cuce, E.; Cuce, P. M.; Wood, C. J.; Riffat, S. B. Toward aerogel based thermal superinsulation in buildings: A comprehensive review. *Renewable Sustainable Energy Rev.* **2014**, *34*, 273–299, DOI: 10.1016/j.rser.2014.03.017.

(12) Thapliyal, P. C.; Singh, K. Aerogels as promising thermal insulating materials: An overview. *J. Mater.* **2014**, *2014*, 1–10, DOI: 10.1155/2014/127049.

(13) Jelle, B. P.; Baetens, R.; Gustavsen, A. Aerogel insulation for building applications. *The Sol-Gel Handbook* **2015**, *3-3*, 1385–1412, DOI: 10.1002/9783527670819.ch45.

(14) Hurwitz, F. I.; Gallagher, M.; Olin, T. C.; Shave, M. K.; Ittes, M. A.; Olafson, K. N.; Fields, M. G.; Guo, H.; Rogers, R. B. Optimization of alumina and aluminosilicate aerogel structure for high-temperature performance. *Int. J. Appl. Glass Sci.* **2014**, *5*, 276–286, DOI: 10.1111/ijag.12070.

(15) Folgar, C.; Folz, D.; Suchicital, C.; Clark, D. Microstructural evolution in silica aerogel. *J. Non-Cryst. Solids* **2007**, *353*, 1483–1490, DOI: 10.1016/j.jnoncrysol.2007.02.047.

(16) Walker, R. C.; Potochniak, A. E.; Hyer, A. P.; Ferri, J. K. Zirconia aerogels for thermal management: Review of synthesis, processing, and properties information architecture. *Adv. Colloid Interface Sci.* **2021**, *295*, 102464, DOI: 10.1016/J.CIS.2021.102464.

(17) Studart, A. R.; Gonzenbach, U. T.; Tervoort, E.; Gauckler, L. J. Processing routes to macroporous ceramics: A review. *J. Am. Ceram. Soc.* **2006**, *89*, 1771–1789, DOI: 10.1111/j.1551-2916.2006.01044.x.

(18) Sai, H.; Xing, L.; Xiang, J.; Zhang, F.; Cui, L.; Liang, X.; Song, B.; Zhao, C.; Li, Z. Effects of surfactants on the synthesis of silica aerogels prepared by ambient pressure drying. *Key Eng. Mater.* **2012**, *512-515*, 1625–1630, DOI: 10.4028/www.scientific.net/KEM.512-515.1625.

(19) Zarzycki, J.; Prassas, M.; Phalippou, J. Synthesis of glasses from gels: The problem of monolithic gels. *J. Mater. Sci.* **1982**, *17*, 3371–3379, DOI: 10.1007/BF01203507.

(20) Rezaee, S.; Ranjbar, K.; Kiasat, A. R. The effect of surfactant on the sol–gel synthesis of alumina-zirconia nanopowders. *Ceram. Int.* **2018**, *44*, 19963–19969, DOI: 10.1016/j.ceramint.2018.07.263.

(21) Jung, H. N. R.; Han, W.; Cho, H. H.; Park, H. H. Effect of cationic and non-ionic surfactants on the microstructure of ambient pressure dried zirconia aerogel. *Mater. Express* **2017**, *7*, 291–298, DOI: 10.1166/mex.2017.1371.

(22) Ruckenstein, E.; Nagarajan, R. Critical micelle concentration. A transition point for micellar size distribution. *J. Phys. Chem.* **1975**, *79*, 2622–2626, DOI: 10.1021/j100591a010.

(23) Vareda, J. P.; Maximiano, P.; Cunha, L. P.; Ferreira, A. F.; Simões, P. N.; Durães, L. Effect of different types of surfactants on the microstructure of methyltrimethoxysilane-derived silica aerogels: A combined experimental and computational approach. *J. Colloid Interface Sci.* **2018**, *512*, 64–76, DOI: 10.1016/j.jcis.2017.10.035.

(24) Walker, R. C.; Stokes, J. L.; Hurwitz, F. I.; Guo, H.; Ferri, J. K. Optimizing surfactant templating of yttria-stabilized zirconia aerogels for high-temperature appli-

cations: Effect of cationic surfactant. *Microporous Mesoporous Mater.* **2022**, *330*, 111577, DOI: https://doi.org/10.1016/j.micromeso.2021.111577.

(25) Perissinotto, A.; Awano, C.; De Vicente, F.; Donatti, D.; Mesquita, A.; Da Silva, L.; Vollet, D. Structure and Diffuse-Boundary in Hydrophobic and Sodium Dodecyl Sulfate-Modified Silica Aerogels. *Microporous Mesoporous Mater.* **2015**, *223*, 196–202, DOI: 10.1016/j.micromeso.2015.11.017.

(26) Chen, D.; Wang, X.; Ding, W.; Zou, W.; Zhu, Q.; Shen, J. Silica aerogel monoliths derived from silica hydrosol with various surfactants. *Molecules* **2018**, *23*, DOI: 10.3390/molecules23123192.

(27) Huo, W.-L.; Zhang, X.-Y.; Chen, Y.-G.; Lu, Y.-J.; Liu, W.-T.; Xi, X.-Q.; Wang, Y.-L.; Xu, J.; Yang, J.-L. Highly Porous Zirconia Ceramic Foams with Low Thermal Conductivity from Particle-Stabilized Foams. *J. Am. Ceram. Soc.* **2016**, *99*, 3512–3515, DOI: https://doi.org/10.1111/jace.14555.

(28) Sarawade, P. B.; Shao, G. N.; Quang, D. V.; Kim, H. T. Effect of various structure directing agents on the physicochemical properties of the silica aerogels prepared at an ambient pressure. *Appl. Surf. Sci.* **2013**, *287*, 84–90, DOI: https://doi.org/10.1016/j.apsusc.2013.09.072.

(29) Cao, S.; Yao, N.; Yeung, K. Synthesis of freestanding silica and titania-silica aerogels with ordered and disordered mesopores. *J. Sol-Gel Sci. Technol.* **2008**, *46*, 323–333, DOI: 10.1007/s10971-008-1701-8.

(30) Hurwitz, F. I.; Rogers, R. B.; Guo, H.; Garg, A.; Olson, N. S.; Phan, D.; Cashman, J. L. Phase development and pore stability of yttria- and ytterbia-stabilized zirconia aerogels. *J. Am. Ceram. Soc.* **2020**, DOI: 10.1111/jace.17376.

(31) Olson, N. S.; Hurwitz, F. I.; Guo, H.; Madden, N. J.; Stokes, J. L.; Rogers, R. B.;

Krogstad, J. A. Enhanced thermal stability of high yttria concentration YSZ aerogels. *J. Am. Ceram. Soc.* **2021**, *104*, 4190–4202, DOI: 10.1111/jace.17792.

(32) Marcolongo, J. P.; Mirenda, M. Thermodynamics of Sodium Dodecyl Sulfate (SDS) Micellization: An Undergraduate Laboratory Experiment. *J. Chem. Educ.* **2011**, *88*, 629–633, DOI: 10.1021/ed900019u.

(33) Mukerjee,; Pasupati,; Mysels,; Karol, *Critical micelle concentrations of aqueous surfactant systems*; 1971; pp 1–222, DOI: 10.6028/NBS.NSRDS.36.

(34) He, Z.; Alexandridis, P. Micellization Thermodynamics of Pluronic P123 (EO20PO70EO20) Amphiphilic Block Copolymer in Aqueous Ethylammonium Nitrate (EAN) Solutions. *Polymers* **2017**, *10*, 32, DOI: 10.3390/polym10010032.

(35) Brunauer, S.; Emmett, P. H.; Teller, E. Adsorption of gases in multimolecular layers. *J. Am. Ceram. Soc.* **1938**, *60*, 309–319, DOI: 10.1021/ja01269a023.

(36) Barrett, E. P.; Joyner, L. G.; Halenda, P. P. The determination of pore volume and area distributions in porous substances. I. Computations from nitrogen isotherms. *J. Am. Ceram. Soc.* **1951**, *73*, 373–380, DOI: 10.1021/ja01145a126.

(37) Rabiei, M.; Palevicius, A.; Monshi, A.; Nasiri, S.; Vilkauskas, A.; Janusas, G. Comparing methods for calculating nano crystal size of natural hydroxyapatite using X-ray diffraction. *Nanomaterials* **2020**, *10*, 1–21, DOI: 10.3390/nano10091627.

(38) Witz, G.; Shklover, V.; Steurer, W.; Bachegowda, S.; Bossmann, H. P. Phase evolution in yttria-stabilized zirconia thermal barrier coatings studied by rietveld refinement of X-ray powder diffraction patterns. *J. Am. Ceram. Soc.* **2007**, *90*, 2935–2940, DOI: 10.1111/J.1551-2916.2007.01785.X.

(39) Thanitwatthanasak, S.; Sagis, L. M.; Chitprasert, P. Pluronic F127/Pluronic P123/vitamin E TPGS mixed micelles for oral delivery of mangiferin and quercetin:

Mixture-design optimization, micellization, and solubilization behavior. *J. Mol. Liq.* **2019**, *274*, 223–238, DOI: https://doi.org/10.1016/j.molliq.2018.10.089.

(40) Kurahashi, M.; Kanamori, K.; Takeda, K.; Kaji, H.; Nakanishi, K. Role of block copolymer surfactant on the pore formation in methylsilsesquioxane aerogel systems. *RSC Adv.* **2012**, *2*, 7166–7173, DOI: 10.1039/C2RA20799K.

(41) Zhao, D.; Feng, J.; Huo, Q.; Melosh, N.; Fredrickson, G.; Chmelka, B.; Stucky, G. Triblock Copolymer Syntheses of Mesoporous Silica With Periodic 50 to 300 Angstrom Pores. *Science (New York, N.Y.)* **1998**, *279*, 548–52, DOI: 10.1126/science.279.5350.548.

(42) Li, W.; Han, Y. C.; Zhang, J. L.; Wang, L. X.; Song, J. Thermodynamic modeling of CTAB aggregation in water-ethanol mixed solvents. *Colloid J.* **2006**, *68*, 304–310, DOI: 10.1134/S1061933X06030069.

Tables

Table 1: Molar ratios of surfactant to inorganic precursors. Molar ratios of the surfactants, SDS and P-123, to the inorganic precursors, zirconium and yttrium, in the aerogel formulations at concentrations of 0.5x, 2x, and 3x the CMC.

		Molar Ratios		
Surfactant	**CMC (M)**	**0.5x**	**2x**	**3x**
SDS	1×10^{-3}	6×10^{-4}	2×10^{-3}	3×10^{-3}
P-123	3×10^{-4}	2×10^{-4}	7×10^{-4}	1×10^{-3}

Table 2: Average crystallite size of YSZ aerogels with various surfactants and heat-treatment conditions. Average crystallite size values (Å) for YSZ aerogels with varying levels of SDS and P-123 at 600°C, 1000°C, and 1100°C determined through XRD and TEM analysis. Four different equations were used to determine the crystallite size following XRD analysis.

Surfactant	**Temperature (°C)**	**Crystallite Size via XRD (Å)**	**Crystallite Size via TEM (Å)**
0x Surfactant	600	55 ± 19	-
	1000	246 ± 20	-
	1100	529 ± 39	364 ± 161
0.5x SDS	600	58 ± 1	-
	1000	237 ± 23	-
	1100	535 ± 19	411 ± 176
2x SDS	600	54 ± 14	-
	1000	197 ± 11	-
	1100	605 ± 9	-
3x SDS	600	56 ± 22	-
	1000	244 ± 9	-
	1100	535 ± 19	355 ± 128
0.5x P-123	600	58 ± 25	-
	1000	202 ± 7	-
	1100	349 ± 3	355 ± 135
2x P-123	600	54 ± 13	-
	1000	200 ± 16	-
	1100	579 ± 18	-
3x P-123	600	57 ± 24	-
	1000	198 ± 5	-
	1100	517 ± 32	347 ± 173

Figures and Figure Captions (to be printed in color)

All figures to be printed in color.

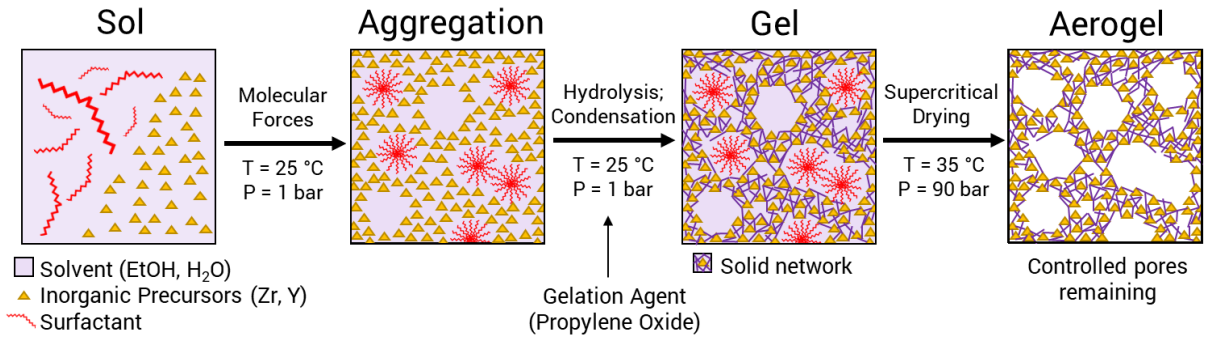

Scheme 1: Surfactant templating during aerogel synthesis. Following formulation of the aerogel sol, precursor particles aggregate around surfactant micelles, gelling to form a solid network. Surfactants are removed from the aerogel, either through washing, supercritical drying, or heat-treatment, leaving behind controllable, uniform pores.

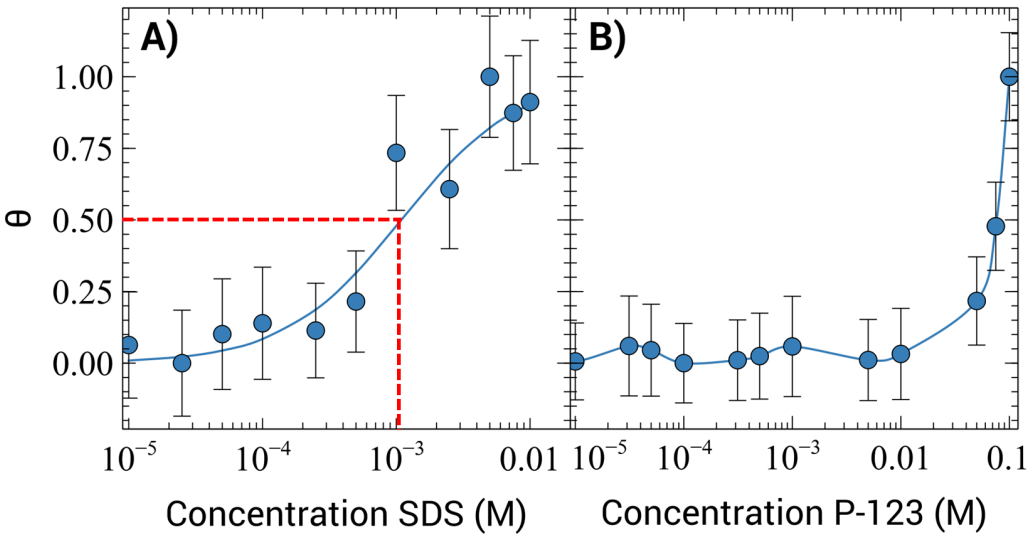

Figure 1: Theta (θ) as a function of surfactant concentration to determine CMC. θ values, defined as (R - R_{min})/(R_{max} - R_{min}) where R is the hydrodynamic radius, for concentrations (M) of the surfactants A) SDS and B) P-123. The critical micelle concentration (CMC) of SDS in the base sol was estimated from 50% θ (red dashed line) to be 1 x 10^{-3} M. The CMC of P-123 used in aerogel formulations was the value for P-123 in water, 3 x 10^{-4} M, as there was not a correlation between hydrodynamic radius and P-123 concentration in this sol.

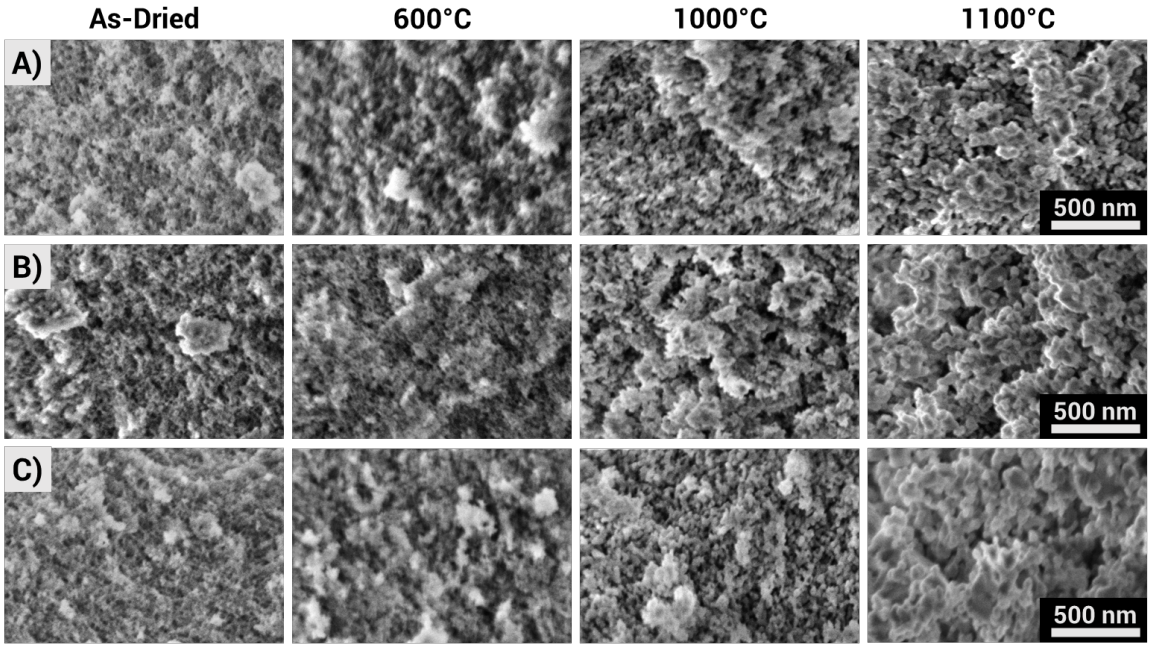

Figure 2: SEM images of YSZ aerogels with various surfactants and heat-treatment conditions. SEM images (80kx magnification) of YSZ aerogels with A) no templating agent, B) 3x SDS, and C) 3x P-123 at four different heat-treatment conditions, left to right, as-dried, 600°C, 1000°C, and 1100°C.

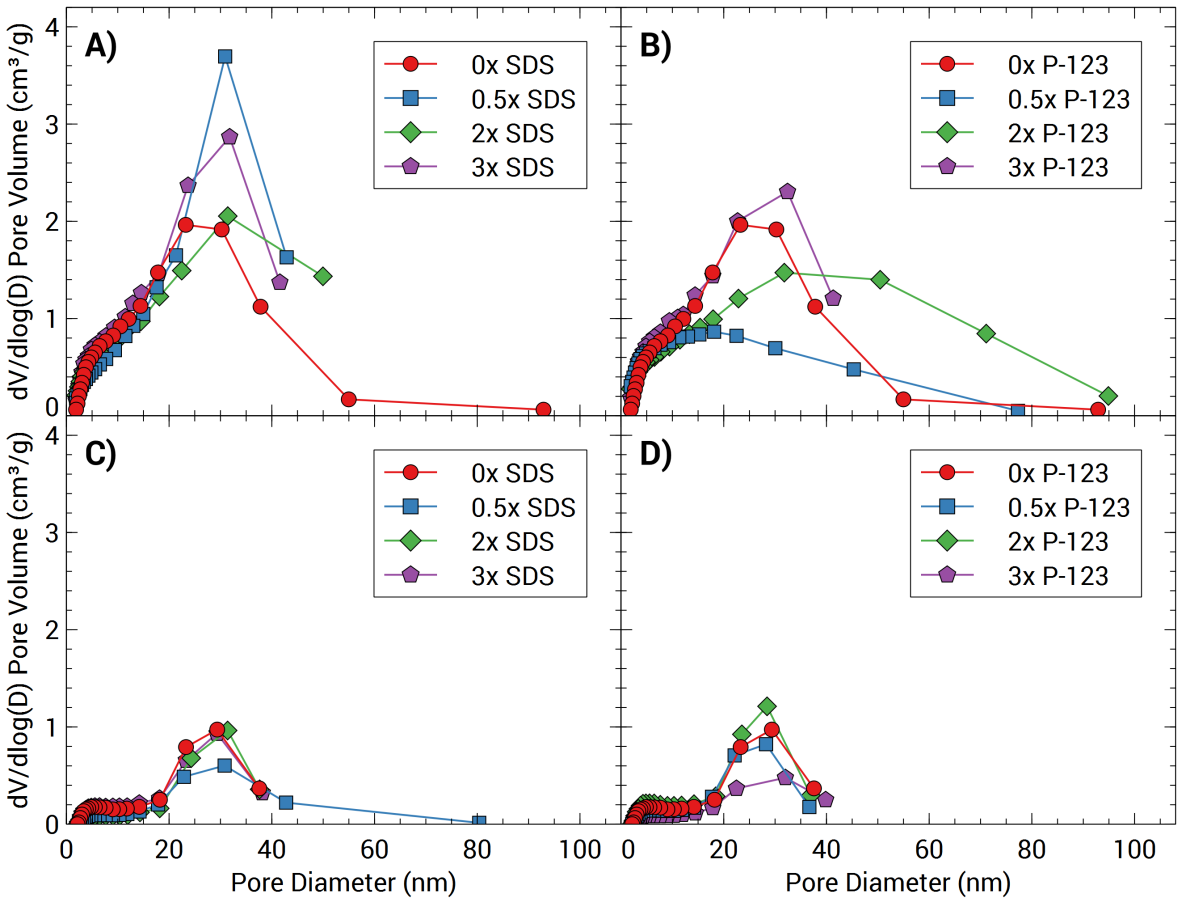

Figure 3: As-dried and heat-treated pore size distributions of YSZ aerogels with various surfactants. Pore size distributions of YSZ aerogels with varying concentrations of SDS (A,C) and P-123 (B,D) that were as-dried (top) and heat-treated at 1000°C (bottom).

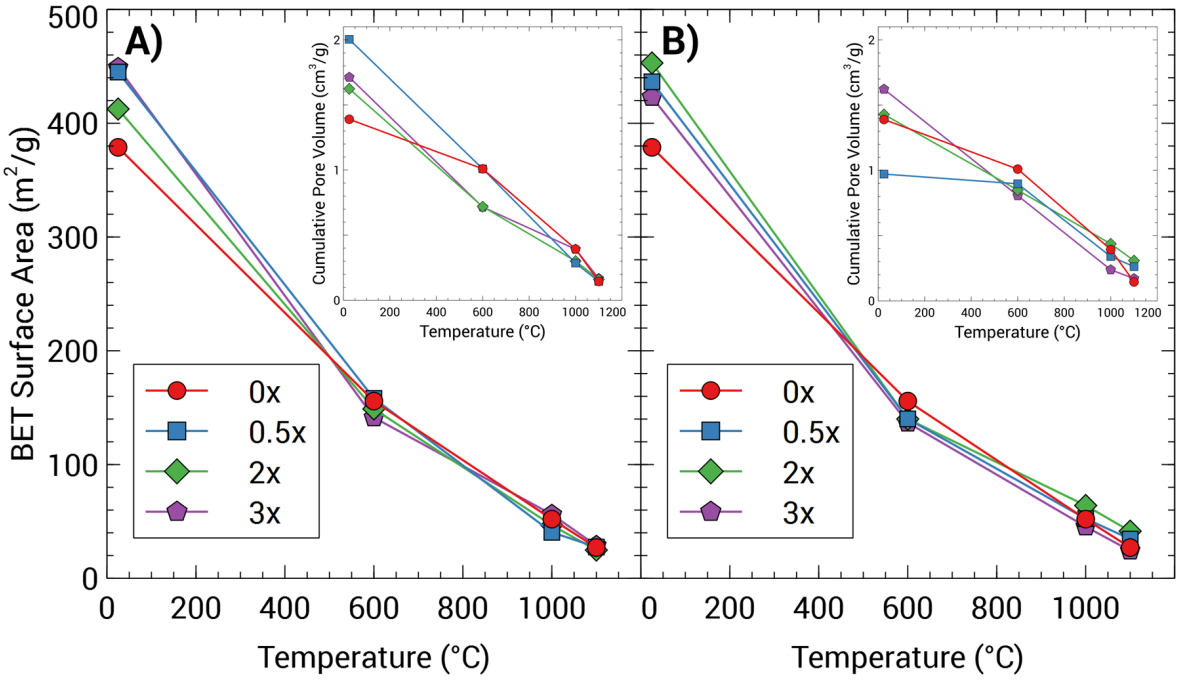

Figure 4: Surface area & pore volume of YSZ aerogels with various surfactants and heat-treatment conditions. BET surface area (m^2/g) and BJH desorption cumulative pore volume (cm^3/g) (inset) for YSZ aerogels with varying concentrations of A) SDS and B) P-123 at as-dried, 600°C, 1000°C, and 1100°C heat-treatment conditions.

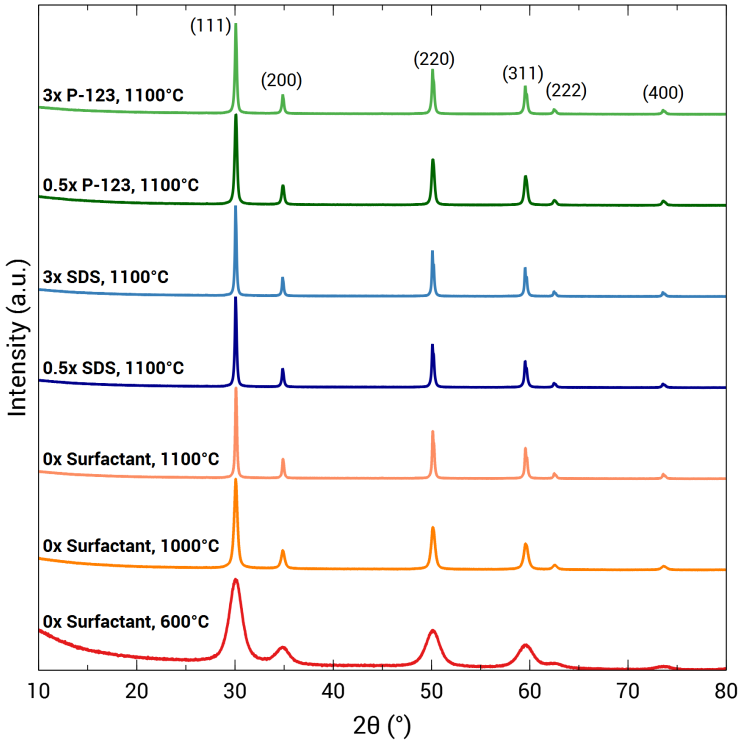

Figure 5: XRD patterns of YSZ aerogels with various surfactants and heat-treatment conditions. XRD patterns from 10° to 80° 2θ for YSZ aerogels without surfactant, with SDS, and with P-123 at various heat-treatment conditions of 600°C, 1000°C, and, primarily, 1100°C. The Miller indices (hkl values) are displayed at the top of the figure.

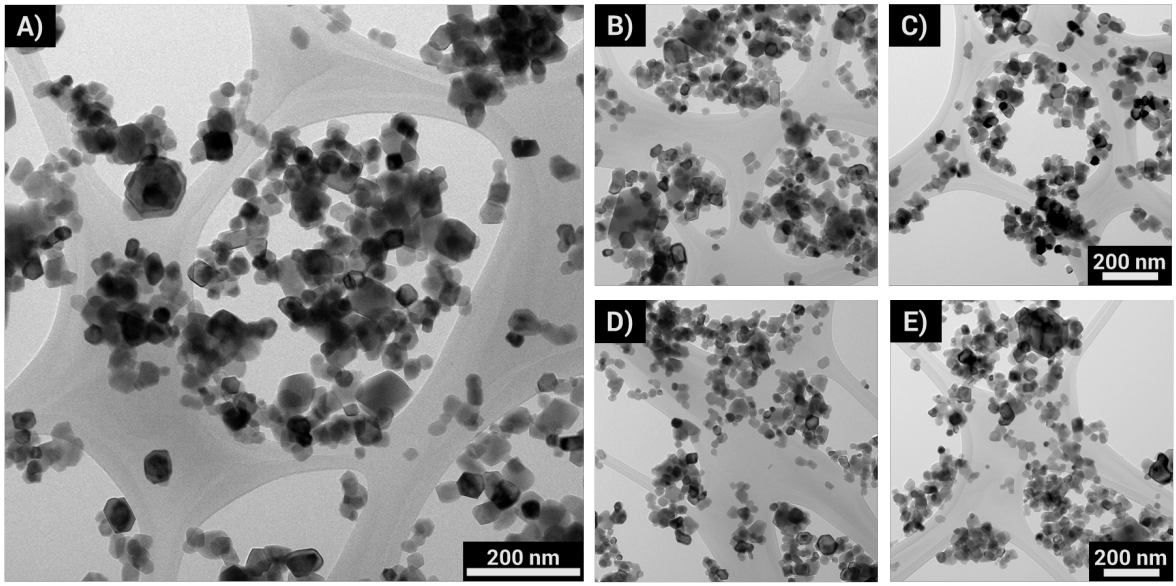

Figure 6: TEM images of YSZ aerogels with various surfactants at 1100°C. TEM images at 58kx magnification for YSZ aerogels at 1100°C with A) no templating agent, B) 0.5x SDS, C) 0.5x P-123, D) 3x SDS, and E) 3x P-123.

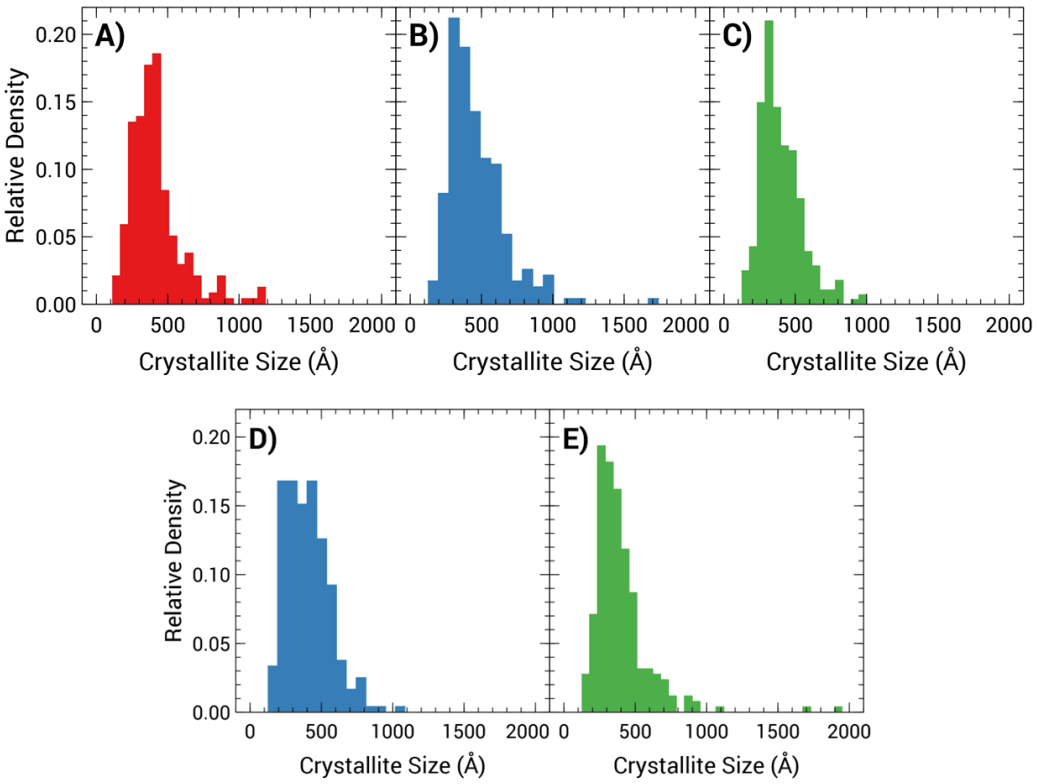

Figure 7: Distribution of crystallite sizes from TEM images. Histograms displaying the distribution of average particle sizes (Å) analyzed via TEM for aerogels at 1100°C with A) no templating agent, B) 0.5x SDS, C) 3x SDS, D) 0.5x P-123,and E) 3x P-123. The Freedman-Diaconis rule was used to determine the bin width. The average crystallite size and standard deviation determined from each sample are displayed in Table 2.